A probabilistic FEM approach for the structural design of glass components

Engineering Fracture Mechanics 282 (2023) 109157

Contents lists available at ScienceDirect

Engineering Fracture Mechanics

journal homepage: www.elsevier.com/locate/engfracmech

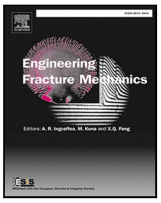

A probabilistic FEM approach for the structural design of glass components

Gregorio Mariggiò, Giulio Ventura, Mauro Corrado *

Department of Structural, Geotechnical and Building Engineering, Politecnico di Torino, Corso Duca degli Abruzzi 24, 10129 Torino, Italy

ARTICLE INFO

MSC:
00-01
99-00

Keywords:
Glass
Structural safety
XFEM
Fracture mechanics
Monte Carlo methods
Failure probability

ABSTRACT

A new probabilistic computational methodology aiming for a safer and optimized design of glass components is proposed, overcoming the drawbacks of the currently employed design approaches. The methodology, which adopts a stress intensity factor-based fracture criterion, can be applied to predict the load bearing capacity associated to any given probability of failure of elements having arbitrary geometry, support conditions and edge flaws scenario.

The main novelty consists in the use of the extended finite element method for the numerical modelling of the structural elements, taking advantage of its intrinsic capability to deal with multiple cracks without adapting the mesh topology and the possibility to directly evaluate the stress intensity factor at the tip of the cracks without any post-processing procedure. Besides, because of the stochastic nature of the problem, where the flaws size is the random variable, the Monte Carlo method is used to obtain the cumulative distribution function of the failure load, from which the load bearing capacity is derived.

Several case studies are reported to demonstrate the accuracy and reliability of the method. It is also shown that, depending on the stress gradient along the glass component, the developed method provides load carrying capacities larger than the predictions of a stress-based approach, by an extent variable between 21% and 83%.

1. Introduction and state-of-the-art

The fracture stress of glass varies widely between 20 and 200 MPa [1], depending on a variety of factors such as the load history [2], the surface condition [3,4], the element's size [5], the environmental conditions [6], the point of the origin of failure (along the edge or on the surface), the type of edge processing [7,8], the presence of thermal treatments [9]. Griffith-like surface flaws cause the brittle failure in glass [10], and their random distribution results in a large scatter in fracture strength and location of failure. Flaws and scratches appear during the manufacturing process, as well as during handling, assembly, everyday use and maintenance [11]. As a result, not only across plates from various production batches, but even within the same batch, flaw characteristics and failure stress magnitudes vary dramatically. The glass flaws depth typically ranges from 20 μm to 200 μm [12]. However, accidental impacts or vandalism might result in more serious damage and much deeper flaws.

Despite the large scatter of the glass strength, several design methods have been proposed. To simplify, they can be divided into two main groups: the methods adopted in the European design standards and those used in the North American design standards.

The European standards EN16612:2019 [13] and CEN/TS 19100-1:2021 [14] propose a stress-based design approach, for which the structural integrity is assessed by comparing the maximum bending stress, σ_{max}, with the design bending strength, $f_{g;d}$:

$$\sigma_{max} \leq f_{g;d} \tag{1}$$

* Corresponding author.
E-mail address: mauro.corrado@polito.it (M. Corrado).

https://doi.org/10.1016/j.engfracmech.2023.109157
Received 8 October 2022; Received in revised form 10 January 2023; Accepted 21 February 2023
Available online 25 February 2023

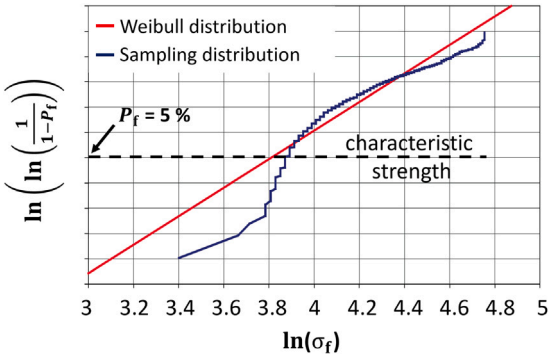

Fig. 1. Cumulative Weibull distribution of the failure stress.
Source: Adapted from [13].

According to EN16612:2019 [13], for annealed glass of any composition, the design value of bending strength is:

$$f_{g;d} = \frac{k_e k_{mod} k_{sp} f_{g;k}}{\gamma_{M;A}} \tag{2}$$

where $f_{g;k} = 45$ MPa is the characteristic value of the bending strength (5% fractile); $\gamma_{M;A}$ is the material partial factor that ranges from 1.6 to 1.8; k_e, k_{sp} and k_{mod} are the strength reduction factors. k_e and k_{sp} take into account the edge and surface finishing, while k_{mod} the load duration. An experimental campaign, involving 741 panes of 6 mm float glass, was carried out according to EN 1288-2 [15] to provide the characteristic glass strength $f_{g;k}$ [13]. The 741 failure stress measurements σ_f were analized statistically, and the $f_{g;k}$ value was derived using the two-parameter Weibull distribution for a probability of failure $P_f = 5\%$, as shown in Fig. 1. However, the sampling distribution is clearly non-linear and poorly fitted by the Weibull distribution. As a result, the confidence intervals of the Weibull parameters are rather broad, and the prediction of extremely low risk levels is uncertain [13].

The stress-based design approach is widely used because of its outstanding simplicity, although it has some drawbacks. The first weakness is that it relies on the bending strength which is not a true material property, as it depends on the flaws size distribution, the fracture toughness, the test setup, as well as the specimen size and geometry [16]. Secondly, when using a deterministic approach, large safety factors need to be introduced for a safe design. However, it is worth noticing that a high safety factor does not necessarily imply a low level of risk, as its influence might be offset by the presence of greater uncertainties in the design environment [17]. In addition, the stress-based design approach assumes that the point of origin of failure coincides with the point of maximum stress, condition that rarely happens in glass [18]. Because of the large scatter in fracture strength and failure origin, a probabilistic approach should be adopted. Recent studies have enhanced the reliability of the semi-probabilistic (level I) method for the design of glass components. For instance, the findings by Ballarini et al. [19] have contributed to reduce the partial safety factors for the structural design of glass by using a generalized distribution of the Weibull type. However, the obtained results can be used only when the maximum tensile stress acts far from the edges. In addition, Lamela et al. [20] showed that the Weibull distribution functions of the glass strength are quite similar under different types of testing.

The American National Standard Practice for Determining Load Resistance of Glass in Buildings, ASTM E1300-16 [21], adopts the model proposed by Beason and Morgan [22,23] for the prediction of the load bearing capacity of glass components. ASTM E1300-16 only applies to vertical and sloped glazing having rectangular shape exposed to a uniform lateral load, such as wind load, snow load and self-weight, with a total combined magnitude less than or equal to 10 kPa. The standard shall not apply to other elements such as, for example, balustrades, glass floor panels, aquariums, structural glass members and glass shelves. Unlike in the European design method, the structural integrity assessment is based on loads rather than stresses. In fact, the structural integrity in ASTM E1300-16 is evaluated by comparing the uniform lateral load q with the load resistance LR which is the load associated to a breakage probability less than or equal to 0.8%:

$$q \leq LR = NFL \cdot GTF \tag{3}$$

being NFL the non-factored load and GTF the glass type factor. The GTF factors are listed in tables function of the glass type and the load duration, whereas the NFL values can be obtained from charts reported in ASTM E1300-16. The NFL parameter is obtained for a load duration of 3 s and depends on support conditions, plate size and plate thickness. The NFL charts were developed using the glass failure prediction model of Beason and Morgan [22,23], who used the Weibull statistics [24] to represent the probability of failure P_f for glass:

$$P_f = 1 - e^{-B} \tag{4}$$

According to Beason and Morgan [23], B reflects the risk of failure and depends on the magnitude and duration of the surface tensile stresses in the plate, the surface area of the plate exposed to tensile stress, and the geometry and orientation of the surface flaws. For general cases, B is computed as follows:

$$B = \check{k} \int_A \left[\check{c}\sigma_{eq,max}(q, x, y)\right]^{\check{m}} \mathrm{d}A \tag{5}$$

where $\sigma_{eq,max}(q, x, y)$ is the maximum equivalent principal stress as a function of the lateral load q and the coordinates (x, y) of the point on the glass surface; $\check{c}$ is the 'biaxial stress correction factor' which is function of the minimum to maximum principal stress ratio; A is the surface area of the plate; $\check{k}$ and $\check{m}$ are the so-called 'surface flaw parameters' which reflect the character of glass plate surface flaws. The non-factored load NFL can be obtained by Eq. (4) once the probability of failure, the support and load conditions, the plate size and thickness, and the surface flaw parameters $\check{k}$ and $\check{m}$ are defined. In ASTM E1300-16, it was assumed $\check{m} = 7$ and $\check{k} = 2.86 \times 10^{-17}$ mm^{12} N^{-7}. According to ASTM E1300-16, these flaw parameters refer to the surface strength of weathered window glass that has undergone in-service conditions for approximately 20 years [21]. The narrow range of application of the standard is due to the fact that the parameters $\check{m}$ and $\check{k}$ have been obtained, and are therefore reliable, only for the case of vertical or sloped glazing in buildings. To summarize, in ASTM E1300-16 the load-carrying capacity of glass plates is evaluated taking into account the actual surface flaw condition and the effect of the plate's size. However, the acceptable probability of failure cannot be set, and the field of application is restricted to vertical and sloped glazing in buildings subjected to uniform lateral load.

Because of the narrow range of application of ASTM E1300 and the weaknesses of the stress-based design approach, new models, more flexible and suitable to be applied for several load and support conditions, should be developed. These models should account for a variety of glass surface scenarios, so that severe surface cracking or specific surface conditions detected by quality control procedures may be included. A reliable and less conservative design method would reduce costs and emissions involved in manufacturing glass components. Besides, the models should be robust, intuitive and easy to use, with few parameters having a clear physical meaning. Additionally, they should be based on the real physical mechanism determining the strength of glass, i.e. the micro-cracks distribution, which is independent of the test configuration and the element size. For this reason, the cracks distribution should be provided after the manufacturing process, and its evolution should be predicted and monitored during storage, assembly, and service stages of glass. Even though some methods for crack and scratch detection have been recently developed, such as those based on microscope inspection techniques [25], thermal stress-induced light scattering techniques [26] and deep learning techniques [27], additional efforts are needed in order to detect and measure the crack size along the edges and on the surface of glass components. In addition, special attention should be paid to the edge flaw condition, since it is one of the main parameters influencing the strength of glass [28], with particular regard to in-plane loaded structural elements, such as glass beams and façade mullions. The edge strength is also relevant in secondary construction elements, such as windows, that may be subjected to significant tensile stress along the edges as result of thermal actions [29], and bolted connections which are subjected to stress concentrations along the hole's edge.

In the present work, a new numerical methodology for the design of annealed glass components is proposed and tested. The method can be used on any flat glass component under in-plane static loads and it adopts a stress intensity factor-based fracture criterion for the prediction of the failure load. This method assumes that edge cracks are Pareto distributed and makes use of the eXtended Finite Element Method (XFEM) [30] for the explicit introduction of cracks in the computational model and the calculation of the stress intensity factors at the tip of each crack. In addition, Monte Carlo simulation is used to obtain the probability density function of the failure load. The model takes into account the size effect on the glass strength and the interaction among cracks for the evaluation of the stress intensity factors, whereas it does not consider the stress corrosion effect.

2. New proposed computational methodology

Glass is a brittle material that fails when the critical value of the stress intensity factor is achieved at the tip of any flaw. The achievement of the failure condition is determined by a complex interplay between the flaw size distribution and the internal stress distribution, such that the critical crack, i.e. the one having the maximum value of the stress intensity factor, is not always placed in the point exhibiting the maximum tensile stress. For a crack subjected to pure Mode I, the fracture criterion is expressed as follows:

$$K_I = K_{IC} \tag{6}$$

where K_I is the Stress Intensity Factor (SIF) and K_{IC} denotes the value of the critical stress intensity factor, also known as fracture toughness [31]. Unlike the bending strength $f_{g;k}$, K_{IC} is a material property, and its value for soda-lime silica glass is estimated to be around 0.75 MPa m$^{1/2}$ [32].

Let us consider a deformable body with a crack of size a, subjected to a remote uniform stress state σ_{yy} applied normally to the plane of the crack, as shown in Fig. 2. The relationship between the fracture toughness K_{IC}, the failure stress $\sigma_{yy,f}$ and the crack size a is derived from linear elastic fracture mechanics:

$$K_{IC} = Y \sigma_{yy,f} \sqrt{\pi a} \tag{7}$$

where Y is a positive dimensionless geometrical factor depending on the aspect ratios of the structural element wherein the crack is placed, the location of the crack (inner or edge crack), and the flaw shape. For instance, Y approaches 1.12 for isolated straight-fronted edge cracks, remotely applied tensile stress (i.e. $H/W \geq 2$), and very small crack length (i.e. $a/W \leq 0.03$), as reported in the handbook by Tada et al. [33].

Yankelevsky [34] developed a numerical method to predict the surface strength of rectangular glass plates under bending for an arbitrary acceptable probability of failure. To fully exploit the bending strength of the glass plate, Yankelevsky [34] included a flaws population on the plate surface, from which the failure stress distribution could be derived. According to the method, the surface of the glass plate is divided into 1 cm^2 unit cells, and a crack is placed in each cell. The crack size a is chosen randomly from a truncated exponential probability distribution. Then, the failure stress $\sigma_{yy,f}$ on the plate side under tension is calculated according

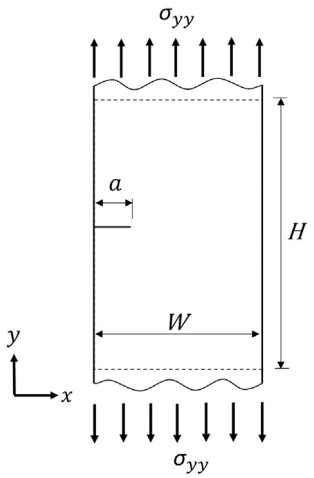

Fig. 2. Edge crack under Mode I loading.

to Eq. (7) for each crack, assuming $Y = 1.12$. As a result, the surface strength of a single plate is represented by the minimum failure stress. A Monte Carlo simulation shall be run on a large sample of thousands of virtual specimens to acquire the probability distribution of both the point of origin of failure and the surface strength.

Kinsella and Persson [1,35] extended the method developed by Yankelevsky [34] to consider multiple flaw populations, arbitrary crack plane orientations and a mixed mode fracture. Due to the results presented in literature works [36–38], Kinsella and Persson [35] adopted for their model the Pareto distribution to describe the statistical population of the depth of surface cracks. The same assumption is made in the present study.

The methodology proposed in this paper adopts the stress intensity factor-based fracture criterion in Eq. (6) for the edge strength prediction of any annealed flat glass component. However, unlike the approaches by Yankelevsky and Kinsella and Persson, the developed computational methodology does not require any post-processing procedure to get the stress intensity factors at the crack tips, as their values are directly provided by the numerical solution. As a consequence, the stress intensity factor values do not depend on assumptions made on the shape function Y. Therefore, the developed methodology is suitable for arbitrary geometries, loads, and boundary conditions, even when closed-form solutions for the stress intensity factor are not available. For example, when cracks are within stress concentration regions or interact with each other. The procedure of the proposed methodology consists of the following six steps:

- The structural element is modelled through the extended finite element method (XFEM);
- A population of edge flaws, which is extracted from a pre-defined statistical distribution function, is randomly applied to the FE model;
- The stress-intensity factors are computed for all the cracks;
- The load carrying capacity is evaluated by equating the maximum stress-intensity factor to the fracture toughness;
- Because of the stochastic nature of the problem, where the size of the edge flaws is the random variable, the Monte Carlo simulation is used to obtain the distribution function of the failure load;
- The critical load referred to a chosen probability of failure is derived.

3. Crack modelling and stress intensity factor evaluation through XFEM

The extended finite element method (XFEM) was proposed by Belytschko and co-workers [39,40] for modelling cracks and crack growth in the FE framework, with no need for the mesh to reproduce the crack geometry. By using XFEM, in fact, a standard FE mesh is first set for the model without taking into account the cracks. Then, cracks are introduced independently of the mesh by enriching the standard displacement approximation with both discontinuous displacement fields along the crack faces [41] and the asymptotic displacement fields at nodes surrounding the crack tips [42].

For a cracked body modelled in the framework of XFEM, the displacement field **u** far from the crack can be approximated by the interpolation of the nodal displacements:

$$\begin{Bmatrix} u(X,Y) \\ v(X,Y) \end{Bmatrix} = \sum_{i \in I} N_i \begin{Bmatrix} u_{0i} \\ v_{0i} \end{Bmatrix} \tag{8}$$

whereas, close to the crack tip and along the crack faces, the standard local displacement approximation shall be enriched with the asymptotic crack tip displacement field [42], which is discontinuous along the crack faces, as shown in Fig. 3:

$$\begin{Bmatrix} u(X,Y) \\ v(X,Y) \end{Bmatrix} = \sum_{i \in I} N_i \begin{Bmatrix} u_{0i} \\ v_{0i} \end{Bmatrix} + \sum_{j \in J_k \cap I} N_j \begin{Bmatrix} u_j^{(\text{tip}\,k)} \\ v_j^{(\text{tip}\,k)} \end{Bmatrix} \tag{9}$$

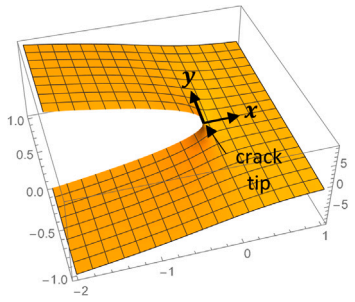

Fig. 3. Asymptotic crack tip displacement field $v^{(tip\,k)}$ close to the crack tip k centred at the origin of the coordinate system x, y.

where I is the set of all nodes in the element, (u_{0i}, v_{0i}) are the standard degrees of freedom at node i, N_i and N_j are the finite element shape functions associated with the node i or j. J_k is the set of nodes that are enriched around the crack tip k and along the crack path; $(u_j^{(\text{tip}\,k)}, v_j^{(\text{tip}\,k)})$ are the values of the asymptotic displacement fields at the node j for the crack tip k.

In the framework of linear elastic fracture mechanics, it is very convenient to adopt the enrichment functions provided by Karihaloo and Xiao [43], which rely on the stress intensity factors at the crack tips. The advantage consists in that the XFEM enrichment variables will be estimates of the stress intensity factors. The general form of the displacement expansions (truncated to the 1st term) near the crack tip for mixed mode in a homogeneous and isotropic material, reads [42]:

$$\begin{Bmatrix} u_j^{(\text{tip}\,k)} \\ v_j^{(\text{tip}\,k)} \end{Bmatrix} = \begin{bmatrix} f_{11} & f_{12} \\ f_{21} & f_{22} \end{bmatrix} \begin{Bmatrix} K_{\text{I}j}^{(\text{tip}\,k)} \\ K_{\text{II}j}^{(\text{tip}\,k)} \end{Bmatrix} \tag{10}$$

where $K_{\text{I}j}$ and $K_{\text{II}j}$ are the Mode I and Mode II stress intensity factors at node j, while f_{11}, f_{12}, f_{21} and f_{22} are the angular functions whose explicit expressions with respect to the polar coordinate system (ρ, ϕ) centred at the crack tip (see Fig. 3) are:

$$\begin{Bmatrix} f_{11} \\ f_{12} \\ f_{21} \\ f_{22} \end{Bmatrix} = \frac{\rho^{1/2}}{2\mu\sqrt{2\pi}} \begin{Bmatrix} (\kappa - \frac{1}{2})\cos\frac{\phi}{2} - \frac{1}{2}\cos\left(-\frac{3}{2}\phi\right) \\ (\kappa + \frac{3}{2})\sin\frac{\phi}{2} - \frac{1}{2}\sin\left(-\frac{3}{2}\phi\right) \\ (\kappa + \frac{1}{2})\sin\frac{\phi}{2} + \frac{1}{2}\sin\left(-\frac{3}{2}\phi\right) \\ -(\kappa - \frac{3}{2})\cos\frac{\phi}{2} - \frac{1}{2}\cos\left(-\frac{3}{2}\phi\right) \end{Bmatrix} \tag{11}$$

being μ and ν the shear modulus and Poisson's ratio of the material, respectively, and $\kappa = (3-4\nu)$ for plane strain or $\kappa = (3-\nu)/(1+\nu)$ for plane stress. The asymptotic displacement fields $(u^{(\text{tip}\,k)}, v^{(\text{tip}\,k)})$ are discontinuous across the crack surface Γ_c. For illustration, the displacement $v^{(\text{tip}\,k)}$ along the y direction is plotted near the crack tip in Fig. 3.

By introducing (10) into (9) it reads:

$$\mathbf{u} = \begin{Bmatrix} u(X,Y) \\ v(X,Y) \end{Bmatrix} = \sum_{i\in I} N_i \begin{Bmatrix} u_{0i} \\ v_{0i} \end{Bmatrix} + \sum_{j\in J_k \cap I} N_j \begin{bmatrix} f_{11} & f_{12} \\ f_{21} & f_{22} \end{bmatrix} \begin{Bmatrix} K_{\text{I}j}^{(\text{tip}\,k)} \\ K_{\text{II}j}^{(\text{tip}\,k)} \end{Bmatrix} = \mathbf{Na} \tag{12}$$

being $\mathbf{a}$ the vector of standard and enriched nodal degrees of freedom including $K_{\text{I}j}^{(\text{tip}\,k)}$ and $K_{\text{II}j}^{(\text{tip}\,k)}$, which are therefore calculated directly without extra post-processing for each node j within the interval J_k by solving the XFEM equilibrium equations.

The XFEM approach has been included in the *X3D* FORTRAN finite element code implemented by Ventura and Benvenuti [44,45], and recently extended by the authors to manage multiple cracks and to perform Monte Carlo simulations. To improve the approximation [46], in the developed code, all the nodes within a distance r from the crack path and tip are enriched, as shown in Fig. 4. As suggested in Ref. [42], in *X3D* a penalty method is employed to enforce constraints to the enriched degrees of freedom, thus improving the stress intensity factors determination. In particular, for each jth enriched node located in the circular region centred at the kth crack tip with radius r_0 (see Fig. 4) the system of linear equations is constrained to return the same value of the stress intensity factors. r_0 should be suitably small, including solely the nodes closest to the crack tips where the asymptotic fields are expected to dominate the solution.

The procedure has been implemented for 4-node quadrilateral elements. In order to ensure that the stiffness matrix is adequately integrated even when the integrand functions are not polynomials (see Eq. (11)), high order Gauss quadratures (8×8 or 20×20 Gauss points) are used over the finite elements whose nodes are enriched.

4. Accuracy of the XFEM-based methodology

Several examples were solved to evaluate the accuracy of the method in assessing the K_{I} and K_{II} values at the crack tips.

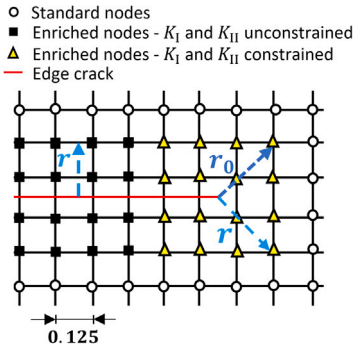

Fig. 4. Edge crack on a uniform mesh. The square and triangular nodes are enriched by the crack tip functions.

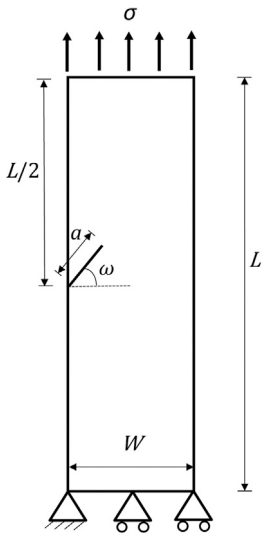

Fig. 5. Sketch of the single edge notched tension specimen.

4.1. Single edge notched tension specimen with an angled-crack

The problem under consideration is a single edge notched tension specimen as shown in Fig. 5. The specimen length is $L = 20$ units, the width is $W = 10$ units, the thickness is $t = 1$ unit, a is the crack length and ω is the crack inclination angle, $\omega = 0°$ denoting pure Mode I cracking. The material is assumed to be linear elastic isotropic ($E = 1$ unit and $\nu = 0.3$), and the problem is idealized as 2D plane stress. A uniaxial stress field, $\sigma = 1$ unit, is applied to the specimen. 2D quadrilateral elements are used to mesh the solid model, with edge size of 0.125 units.

The stress intensity factor is calculated at the crack tip for different crack lengths, and for $\omega = 0°$ and $\omega = 45°$. The numerical integration over the enriched finite elements is performed using 8×8 and 20×20 Gauss points (GP) for $\omega = 45°$, whereas only 8×8 GP are adopted for $\omega = 0°$. The enrichment radius r is set to 0.55, while r_0 (i.e., the radius within which the enriched variables are constrained to be the same) is set to 0.27.

The resulting K_I values for $\omega = 0°$ are reported in Table 1, together with those obtained numerically by Albinmousa et al. [47], herein considered as the reference solution. Tables 2 and 3 list, respectively, the K_I and K_{II} values for $\omega = 45°$, both calculated with *X3D* and according to Albinmousa et al. [47]. In the tables, the error is computed as:

$$Error = \frac{K_{I,X3D} - K_{I,Reference}}{K_{I,Reference}} \tag{13}$$

As it can be seen in Table 1, when $\omega = 0°$, an excellent agreement with the reference solution is maintained for the considered range of crack lengths a. It is important to remark that what matters is the inclination of the crack with respect to the mesh orientation instead of the inclination with respect to the specimen geometry. When $\omega = 0°$, the crack is parallel to one of the side of the finite element, while if $\omega = 45°$ the crack is inclined with regard to the sides of the finite elements, resulting in the increase of the complexity of the mathematical expressions of the integrands of the stiffness matrix, which are far from polynomials. In the latter case, in fact, large errors are obtained, especially for small crack sizes (see Tables 2 and 3), even by increasing the quadrature

Table 1
K_I values for a horizontal edge crack ($\omega = 0°$) in an isotropic elastic plate under tension - 8 × 8 Gauss Points.

a	$K_{I,X3D}$	$K_{I,Ref.}$ [47]	*Error* (%)
0.25	0.94	0.97	−2.7
0.5	1.35	1.4	−3.8
1	2.04	2.10	−2.7
2	3.40	3.44	−1.1
4	7.61	7.46	+1.9
5	11.50	11.15	+3.2

Table 2
K_I values for an inclined edge crack ($\omega = 45°$) in an isotropic elastic plate under tension.

a	8 × 8 Gauss Points		20 × 20 Gauss Points		$K_{I,Ref.}$ [47]
	$K_{I,X3D}$	*Error* (%)	$K_{I,X3D}$	*Error* (%)	
0.25	0.74	+22.2	0.68	+12.8	0.60
0.5	0.97	+11.9	0.96	+10.3	0.87
1	1.37	+7.4	1.36	+6.3	1.28
2	2.06	+3.7	2.02	+1.9	1.98
4	3.81	+5.6	3.79	+5.0	3.61
5	5.19	+9.4	5.12	+8.1	4.74

Table 3
K_{II} values for an inclined edge crack ($\omega = 45°$) in an isotropic elastic plate under tension.

a	8 × 8 Gauss Points		20 × 20 Gauss Points		$K_{II,Ref.}$ [47]
	$K_{II,X3D}$	*Error* (%)	$K_{II,X3D}$	*Error* (%)	
0.25	0.15	−51.9	0.25	−19.5	0.31
0.5	0.36	−19.8	0.36	−17.6	0.44
1	0.58	−11.1	0.57	−11.7	0.65
2	0.95	−5.2	0.92	−7.9	0.99
4	1.72	−2.7	1.70	−3.4	1.76
5	2.22	−2.0	2.20	−2.7	2.26

order to 20 × 20 GP. Additional approaches may be implemented to further improve the solution, such as that based on equivalent polynomials proposed in [48–50] and the blending techniques introduced in [51,52], but these aspects are out of the scope of the present work.

4.2. Stress intensity factor prediction for micro-cracks with coarse mesh

In this example, the minimum crack length that provides an accurate solution in terms of K_I is identified in relation to the mesh size l. For this purpose, a single edge notch tension specimen is considered, whose sketch is shown in Fig. 6. Plane strain conditions are adopted. The specimen has height $H = 30$ mm and width $W = 7.5$ mm. It is subjected to a tensile stress $\sigma = 10$ MPa. The specimen includes a crack whose length a ranges from 10 μm to 100 μm (see Table 4), which are typical sizes for flaws in glass [12]. The problem is solved with a regular mesh of 4-node quadrilateral elements with an edge size set to 0.25 mm. Young's modulus is chosen as 70,000 MPa and Poisson's ratio is taken as 0.25. The enrichment radius is chosen as $r = 0.45$ mm (see Fig. 7). Because of the very small extension of the enriched region, r_0 is set equal to r.

The K_I values obtained with the numerical simulations are listed in Table 4, together with the reference solutions calculated as:

$$K_I = \sigma\sqrt{\pi a}F(a/W) \tag{14}$$

where $F(a/W)$ is calculated for each single crack length a with accuracy better than 0.5%, according to the handbook by Tada et al. [33].

Table 4 shows that, on average, the 20 × 20 Gauss quadrature yields better results than the 8 × 8 Gauss quadrature, confirming the findings of Section 4.1. In particular, in the case of 20 × 20 GP, the error in the estimation of K_I is below 4% for any crack length between 0.02 mm and 0.1 mm (crack length to finite element size between 8% and 40%), while for $a = 0.01$ mm the error is about 15%. For 8 × 8 GP and $a = 0.01$ mm the error increases almost to 26%. In conclusion, the XFEM technique returns accurate K_I values even when the mesh is coarse, unlike the standard FEM approach, which requires a denser mesh to yield a precise stress value in the presence of stress concentrations and singularities.

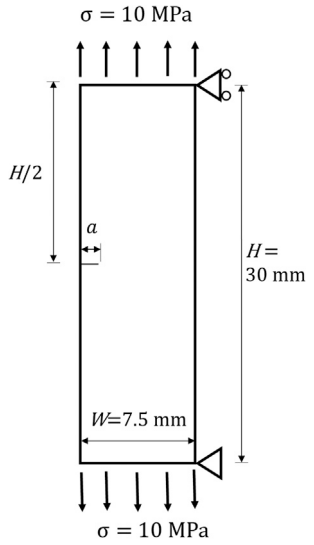

Fig. 6. Sketch of the uniaxial tensile test.

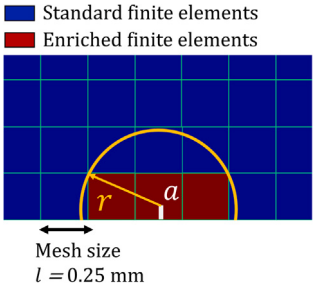

Fig. 7. FE mesh and enriched finite elements, $r = 0.45$ mm.

Table 4
K_I values for a single edge notched tension specimen.

a	8 × 8 Gauss Points		20 × 20 Gauss Points		Reference Solution
(mm)	$K_{I,X3D}$ (MPa mm$^{1/2}$)	*Error* (%)	$K_{I,X3D}$ (MPa mm$^{1/2}$)	*Error* (%)	K_I (Eq. (14)) (MPa mm$^{1/2}$)
0.01	2.51	+26.2	2.28	+14.7	1.99
0.02	2.93	+4.2	2.78	−1.1	2.81
0.025	3.25	+3.4	3.10	−1.4	3.14
0.03	3.62	+5.2	3.31	−3.8	3.44
0.035	3.96	+6.5	3.64	−2.1	3.72
0.04	4.19	+5.4	3.88	−2.4	3.97
0.05	4.44	−0.1	4.40	−1.0	4.44
0.06	4.87	+0.1	4.70	−3.4	4.87
0.065	5.22	+3.1	5.03	−0.7	5.07
0.07	5.62	+6.9	5.32	+1.2	5.26
0.075	5.86	+7.7	5.36	−1.5	5.44
0.08	6.0	+6.8	5.57	−0.9	5.62
0.09	6.04	+1.4	5.95	−0.2	5.96
0.1	6.20	−1.3	6.26	−0.3	6.28

4.3. Multiple interacting edge cracks

In this section the example of three interactive parallel edge cracks in a plate subjected to tensile load is analysed. Auradou et al. [53] showed that the presence of neighbouring cracks modifies the stress field within the body and induces a shielding of the stress at the crack tips. According to Afferrante et al. [16], the statistical distribution of the glass failure stress would change depending on the distribution of cracks, their distances, and their interaction with the geometry and the stress field. As

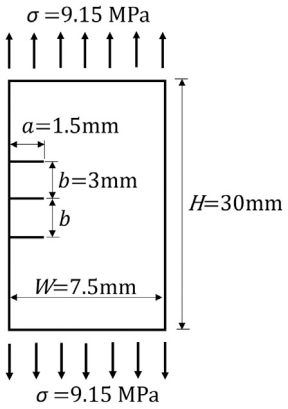

Fig. 8. Parallel cracks in a finite plate under uniaxial tensile load.

Table 5
Stress intensity factors for parallel edge cracks in a finite plate.

Crack	a (mm)	σ (MPa)	K_{LX3D} (MPa m$^{1/2}$)	$K_{\mathrm{I,Reference}}$ [54] (MPa m$^{1/2}$)	*Error* (%)
Outer	1.5	9.15	0.75	0.76	−1.60
Central	1.5	9.15	0.63	0.65	−3.37

a consequence, the correct failure stress distribution can only be obtained through numerical simulations in which the cracks distribution is directly included in the model.

Fig. 8 shows the setup of the virtual specimen, that is analysed in plane strain conditions. A tensile stress $\sigma = 9.15$ MPa is applied to a finite plate with three edge cracks. The plate width is $W = 7.5$ mm, while its height is $H = 30$ mm. The length of the three cracks is $a = 1.5$ mm, and they are far from each other $b = 3$ mm, i.e. twice their length. The mechanical properties and the finite element type and size are the same as for the previous example. The enrichment radii r and r_0 are chosen as 0.50 mm.

K_{I} values for central and outer cracks are listed in Table 5. The error with respect to the numerical solution provided by Jiang et al. [54] is less than 4%.

5. Critical crack and failure stress distributions for uniform and uniaxial stress

Following previous studies [29,35], the population of the size a of edge cracks can be realistically represented by a single Pareto distribution, that is described as [55]:

$$F_{\mathrm{Pareto}}(a) = 1 - \left(\frac{a_0}{a}\right)^c \tag{15}$$

with $a_0 \leq a < \infty$, $a_0 > 0$ and $c > 0$. c is the shape parameter, whilst a_0 is the scale parameter, which represents the smallest edge crack size.

Let us consider a glass plate subjected to uniaxial tensile loading, with a single edge crack of size a perpendicular to the loading and no sub-critical crack growth (see, for example, Fig. 2). The survival probability of the plate is expressed as the probability that the size a is smaller than the critical crack depth a_c:

$$P(a < a_c) = F_{\mathrm{Pareto}}(a_c) = 1 - \left(\frac{a_0}{a_c}\right)^c \tag{16}$$

Supposing now that the glass plate has a random number i of isolated edge cracks, since a_c is constant in case of uniaxial loading perpendicular to the cracks, the survival probability of the plate is the product of the survival probabilities of all cracks:

$$P(a < a_c) = \left[1 - \left(\frac{a_0}{a_c}\right)^c\right]^i \tag{17}$$

Assuming that the real number of defects x is a random variable which follows a Poisson distribution with mean m [56]:

$$F_{\mathrm{Poisson}}(x) = \sum_{i=0}^{x} \frac{e^{-m} m^i}{i!} \tag{18}$$

the survival probability of a random glass plate is now obtained by multiplying the probability $F_{\mathrm{Poisson}}(x)$ from Eq. (18) by the survival probability from Eq. (17):

$$P(a < a_c) = \sum_{i=0}^{x} \frac{e^{-m} m^i}{i!} \left[1 - \left(\frac{a_0}{a_c}\right)^c\right]^i \tag{19}$$

For all possible numbers of cracks the survival probability is:

$$P(a < a_c) = \sum_{i=0}^{\infty} \frac{e^{-m}}{i!} \left\{ m \left[1 - \left(\frac{a_0}{a_c} \right)^c \right] \right\}^i \tag{20}$$

Introducing the definition of the exponential function as an infinite series:

$$e^{\xi} = \sum_{i=0}^{\infty} \frac{1}{i!} \xi^i \tag{21}$$

the survival probability of a glass plate with average number of cracks equal to m becomes:

$$P(a < a_c) = e^{-m a_0^c a_c^{-c}} \tag{22}$$

Finally, by substituting:

$$\lambda = m a_0^c \tag{23a}$$

and

$$\alpha = c \tag{23b}$$

in Eq. (22), the Fréchet cumulative distribution function of the critical edge crack size is obtained:

$$F_{\text{Fréchet}}(a_c) = e^{-\lambda a_c^{-\alpha}} \tag{24}$$

The Fréchet distribution is a special case of the so-called generalized extreme value distribution [57], that find applications in many areas, such as rainfall analysis, seismic analysis, radioactive emissions, strength of materials, insurance and financial matters [58]. In Eq. (24), the exponent $\alpha > 0$ is the shape parameter, while $\lambda > 0$ the scale parameter. The Fréchet distribution is also referred to as Inverse Weibull distribution.

In the same way, Haldimann et al. [59] showed that the strength of glass, under uniaxial tensile loading σ_f, follows the Weibull distribution in Eq. (25a) if the cracks population is represented by a single Pareto distribution:

$$F_{\text{Weibull}}(\sigma_f) = 1 - \exp\left[- \left(\frac{\sigma_f}{\theta} \right)^{\beta} \right] \tag{25a}$$

$$\theta = \frac{K_{IC}}{m^{\frac{1}{\beta}} Y \sqrt{\pi} \sqrt{a_0}}, \qquad \beta = 2c \tag{25b}$$

It is important to remark that Weibull and Fréchet distributions are related to each other by Eqs. (25b) only under the hypothesis of a uniform uniaxial stress field acting perpendicular to the cracks. The relationships in Eqs. (25b) lose their validity in case of arbitrary stress field and gradient.

The Weibull parameters θ and β can be obtained, for instance, by uniaxial tensile tests using small scale glass specimens. Once they are evaluated and the size of the smallest flaw a_0 is assumed, the parameters m and c can be estimated by means of Eq. (25b). Finally, the average number of defects m and the size of the glass specimens can be used to calculate the density of the glass defects. The average number of cracks m and the shape parameter c are true material properties unlike θ and β, which depend on the test setup and the element size.

6. Case studies and discussion

The proposed XFEM-based methodology is now applied to evaluate the load bearing capacity of glass components. The influence of the stress gradient is also studied using four different test configurations: a specimen under uniaxial tensile load, a beam under three point bending, a simply supported beam and a cantilever beam, both subjected to a uniformly distributed load. In addition, a comparative study is conducted to show the difference between the stress-based design approach and the proposed one.

All the considered case studies were analysed in plane stress conditions, adopting the following material properties: $\nu = 0.25$, $E = 70{,}000$ MPa and $K_{\text{IC}} = 0.75$ MPa m$^{1/2}$. Based on the findings of the tests presented in Section 4, the continuum was discretized using a regular and uniform mesh of 4-node quadrilateral elements with edge size $l = 0.25$ mm, cracks parallel to one of the side of the finite element were considered, the enrichment radii were chosen as $r = r_0 = 0.45$ mm, a 20×20 Gauss quadrature rule was adopted over the enriched finite elements. It is to be noted that the edge size of the finite element has been selected in such a way to have the crack length to element size ratio falling within the range 8%–40%, which allows to get very accurate results, as shown in Section 4.2.

6.1. Edge-cracked specimen under uniaxial tensile load

Consider an edge-cracked specimen, as shown in Fig. 9, subjected to uniaxial tensile stress, provided by a uniform distributed load, q, applied at the right and left edges. The specimen has length $L = 30$ mm, height $H = 7.5$ mm and thickness $t = 1$ mm. The specimen includes 29 cracks, which are placed every millimetre. It is assumed that the crack size a follows the Pareto distribution

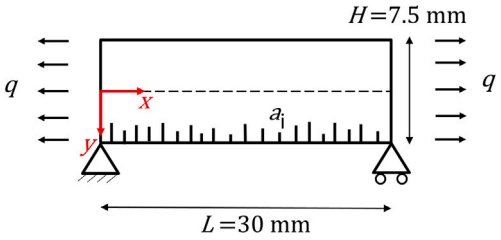

Fig. 9. Specimen under uniaxial tensile load.

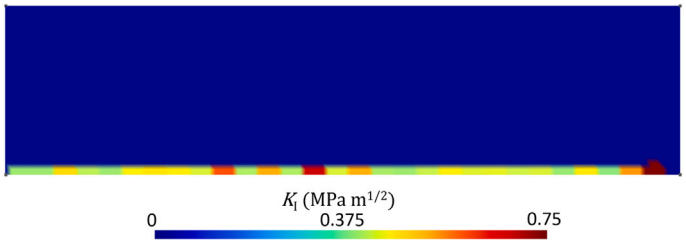

Fig. 10. Specimen under uniaxial tensile load: K_I values at the crack tips for a single simulation.

in Eq. (15) with scale parameter $a_0 = 0.020$ mm and shape parameter $c = 3.0$. The value of the parameter c is chosen based on the findings of the study by Vandebroek et al. [29], where the glass edge strength was investigated experimentally using a four-point bending configuration. The tests, that involved almost 40 specimens with polished edge finishing, showed that the experimental data could be interpolated by a Weibull distribution with shape parameter $\beta \simeq 6$. As a consequence, the Pareto parameter c can be derived using Eq. (25b) as $c = \beta/2$.

The failure load $q_{f,i}$ of the virtual specimen was calculated for $n = 5000$ different simulations, since Yankelevsky [34] showed that this number of simulations guarantees a reliable convergence and repeatable results. In each simulation, the size of the cracks along the bottom side of the specimen varied according to the Pareto distribution. RANDOM_NUMBER() is the FORTRAN function used in *X3D* to extract pseudo-random crack sizes from the Pareto distribution. The failure load was obtained for each simulation by equating the maximum value of K_I to K_{IC}. Fig. 10 shows the K_I values at each of the crack tips for a single simulation.

The computed failure loads, $q_{f,i}$, were ranked in ascending order ($i = 1$ to n) to build an ordered sample with n values and, then, a probability of failure was assigned to each value $q_{f,i}$ of the ordered sample by means of probability estimators $\hat{G}_i$:

$$\hat{G}_i = \frac{i - 0.3}{n + 0.4} \tag{26}$$

The points $(q_{f,i}, \hat{G}_i)$ build the sampling cumulative distribution function of the failure load.

As recalled in Section 5, the statistical population of the failure load, q_f, of a glass specimen having crack sizes Pareto distributed, can be represented by a two parameter Weibull distribution function:

$$F_{\text{Weibull}}(q_f) = 1 - \exp\left[-\left(\frac{q_f}{\hat{\theta}}\right)^{\hat{\beta}}\right] \tag{27}$$

where $\hat{\beta}$ and $\hat{\theta}$ are the Weibull shape and scale parameters, which can be estimated with the moments method [60]:

$$\frac{\Gamma\left(1 + \frac{2}{\hat{\beta}}\right)}{\Gamma^2\left(1 + \frac{1}{\hat{\beta}}\right)} - 1 = \frac{\hat{s}^2_{q_f}}{\hat{\mu}^2_{q_f}} \tag{28a}$$

$$\hat{\theta} = \frac{\hat{\mu}_{q_f}}{\Gamma\left(1 + \frac{1}{\hat{\beta}}\right)} \tag{28b}$$

being $\hat{\mu}_{q_f}$ and $\hat{s}^2_{q_f}$ the sample mean and variance:

$$\hat{\mu}_{q_f} = \frac{\sum_{i=1}^{N} q_{f,i}}{N} \tag{29a}$$

$$\hat{s}^2_{q_f} = \frac{\sum_{i=1}^{N} \left(q_{f,i} - \hat{\mu}_{q_f}\right)^2}{N - 1} \tag{29b}$$

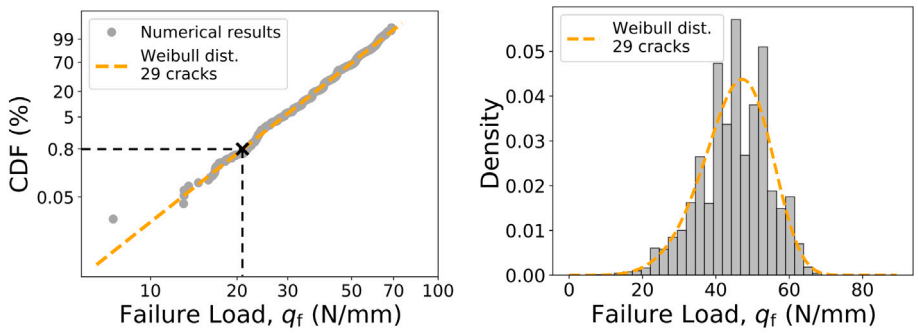

Fig. 11. Weibull distribution of the failure load for the glass specimen under uniaxial tensile load: (a) Linearized cumulative distribution function; (b) Probability density function.

Table 6
Weibull and Fréchet parameters for the glass specimen under uniaxial tensile load.

n. of cracks	Pareto param.		Weibull parameters				Fréchet parameters			
m	a_0 (mm)	c	$\hat{\theta}$ (N/mm)	$\hat{\beta}$	θ (N/mm)	β	$\hat{\lambda}$	$\hat{\alpha}$	λ	α
29	0.02	3.0	48.8	5.7	48.2	6.0	2.4×10^{-4}	3.0	2.3×10^{-4}	3.0

By solving Eq. (28a), using any of a number of standard iterative root-findings procedures, and Eq. (28b), the parameters of the Weibull distribution function of the failure load can be obtained: $\hat{\theta} = 48.8$ N/mm and $\hat{\beta} = 5.7$.

The sampling cumulative distribution function ($q_{f,i}$, $\hat{G}_i$) and the Weibull distribution function of the failure load are plotted into the diagram of Fig. 11(a). The Weibull density function of the failure load is plotted in Fig. 11(b), where it is compared to the histogram whose bars represent the relative number of the failure load, q_f, obtained from the numerical simulations. Even though the histogram is not a smooth function, a reasonable fit of the numerical results is obtained with the Weibull distribution. It is worth noticing that the numerical results plotted in Fig. 11(a) follow a regular two parameter Weibull distribution function, whereas the experimental results in Fig. 1 could be more accurately interpolated by a bilinear and bimodal Weibull distribution, in accordance with the findings of Ballarini et al. [61]. This discrepancy is due to the fact that for the numerical tests the edge cracks were extracted from a single statistical population, whereas the experimental results in Fig. 1 suggest that the initial cracks belong to two different statistical populations, which differ from each other either in the crack shape or in the dispersion of the crack size, or in the two factors combined. In particular, the experimental results indicate that the smallest cracks are more scattered than the biggest ones, which causes the slope of the right tail of the sampling distribution to be lower than that of the left one. However, this difference does not undermine the validity of the numerical approach. It is only a matter of choosing a correct crack size distribution.

The statistical distribution of the size of the critical edge cracks, which represent the point of origin of failure, has been obtained by the numerical results. As clearly shown in Figs. 12(a) and 12(b), the Fréchet distribution provided by Eq. (24) fits the numerical data perfectly. The Fréchet distribution parameters λ and α are calculated by means of the moments method [57]. The estimator for $\hat{\alpha}$ can be obtained by solving the following non-linear equation:

$$\frac{\Gamma\left(1-2\hat{\alpha}^{-1}\right)}{\Gamma^2\left(1-\hat{\alpha}^{-1}\right)} - 1 = \frac{\hat{s}^2_{a_c}}{\hat{\mu}^2_{a_c}} \tag{30}$$

while the parameter $\hat{\lambda}$ can be obtained by solving:

$$\hat{\lambda} = \frac{\hat{\mu}^{\hat{\alpha}}_{a_c}}{\Gamma^{\hat{\alpha}}\left(1-\hat{\alpha}^{-1}\right)} \tag{31}$$

Like the failure load and the critical edge crack size, the fracture origin point is considered a random variable that is predicted by the methodology and shown in the graph of Fig. 13. The point of origin of failure is uniformly distributed since the specimen is subjected to a uniaxial and uniform tensile load.

Finally, in Table 6, the estimated Weibull parameters $\hat{\theta}$ and $\hat{\beta}$ are compared to the experimental ones, θ and β, obtained by Vandebroek et al. [29] and used as input for the numerical procedure. The same is done for the Fréchet parameters α and λ. The good match between the estimated and experimental distribution parameters is another proof of the accuracy and validity of the proposed methodology.

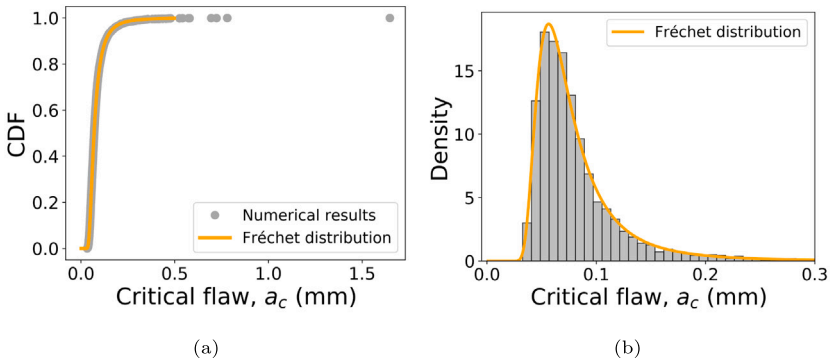

Fig. 12. Fréchet distribution of the critical edge crack size for the glass specimen under uniaxial tensile load: (a) Cumulative distribution function (CDF); (b) Probability density function.

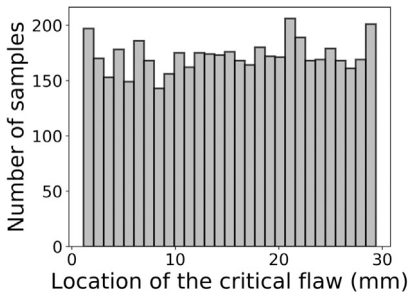

Fig. 13. Location of the critical edge crack for the glass specimen under uniaxial tensile load.

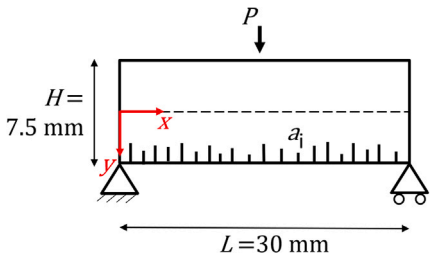

Fig. 14. Sketch of the three point bending test.

6.2. Edge-cracked beam under three point bending

This example involves the edge cracked beam from Section 6.1 subjected to three point bending (Fig. 14). The beam contains 29 edge cracks Pareto distributed ($a_0 = 0.020$ mm and $c = 3.0$) and, just like the previous example, the failure load $P_{f,i}$ was determined for 5000 simulations. The ith failure load corresponds to the load for which $K_I^{max} = K_{IC}$ at one of the 29 edge cracks. For the sake of example, the K_I values at each crack tip for a single simulation are plotted in Fig. 15. The highest values of K_I are obtained near the mid-span of the beam, where the bending moment takes the maximum value.

The failure load values, $P_{f,i}$, were analysed statistically using the Weibull distribution, whereas the critical crack size, a_c, using the Fréchet distribution, as discussed above. The diagrams in Fig. 16 show good agreement between the sampling distribution of the failure load and the Weibull distribution. At the same time, Fig. 17 shows an excellent match between the sampling distribution of the critical crack size and the Fréchet distribution. The Weibull and Fréchet parameters, estimated with the moments method, are: $\hat{\theta} = 83.5$ N and $\hat{\beta} = 6.0$, $\hat{\lambda} = 2.3 \times 10^{-4}$ and $\hat{\alpha} = 2.7$.

The fracture origin coordinate x is normally distributed around the mean $\bar{x} = 15$ mm (Fig. 18) with standard deviation $\sqrt{s_x^2} = 3.25$ mm. However, it is shown that fracture can occur anywhere between $x = 5$ mm and $x = 25$ mm.

By interpolating the sampling cumulative distribution function of the failure load with the Weibull distribution the following load bearing capacity evaluated with a 0.8% probability of failure is obtained: $P_{f,0.008} = 37.55$ N (see Fig. 16(a)).

The design load bearing capacity for the three-point bending test is now estimated through a stress-based failure criterion. First, the glass tensile strength of the beam with 29 cracks must be defined. Based on the outcomes of the previous case study (see

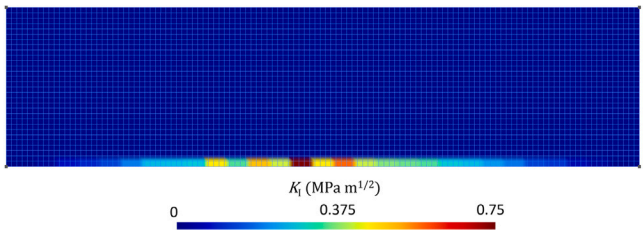

Fig. 15. Beam subjected to three point bending: K_I values at the crack tips for a single example simulation.

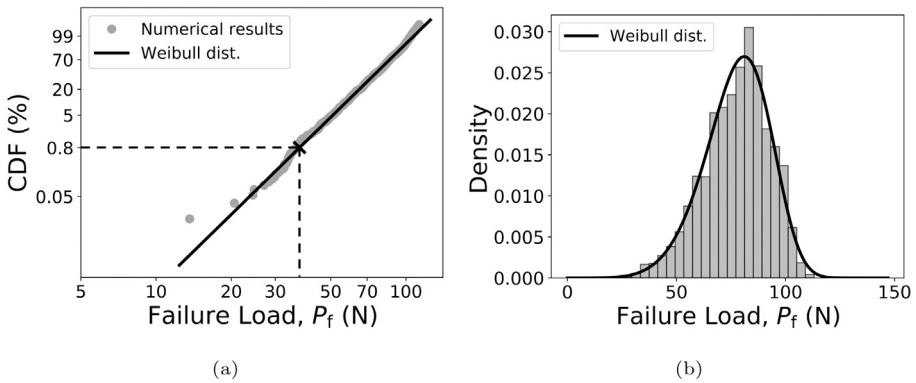

Fig. 16. Weibull distribution of the failure load for the glass beam under three point bending: (a) Linearized cumulative distribution function; (b) Probability density function.

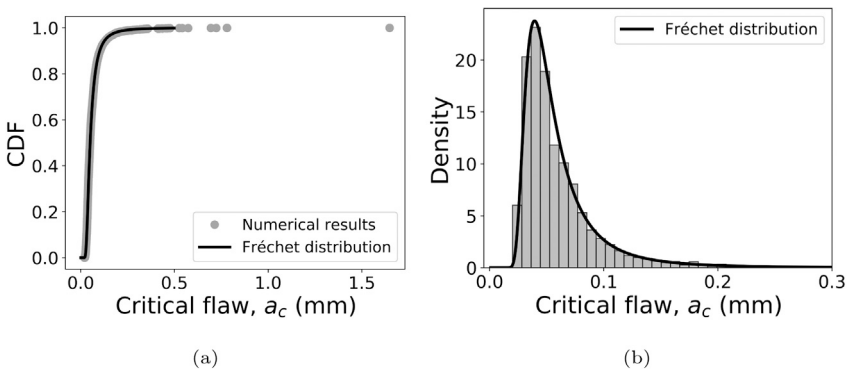

Fig. 17. Fréchet distribution of critical edge crack size for the glass beam with 29 cracks under three point bending: (a) Cumulative distribution function (CDF); (b) Probability density function.

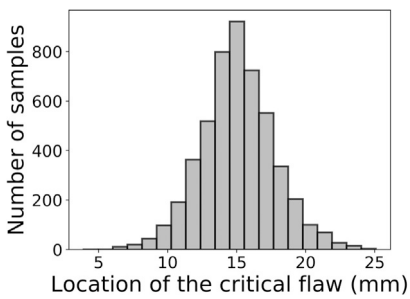

Fig. 18. Location of the critical edge crack for the glass beam under three point bending.

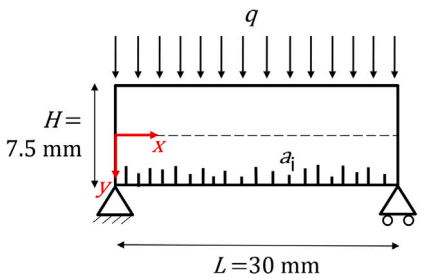

Fig. 19. Simply supported beam under uniformly distributed load.

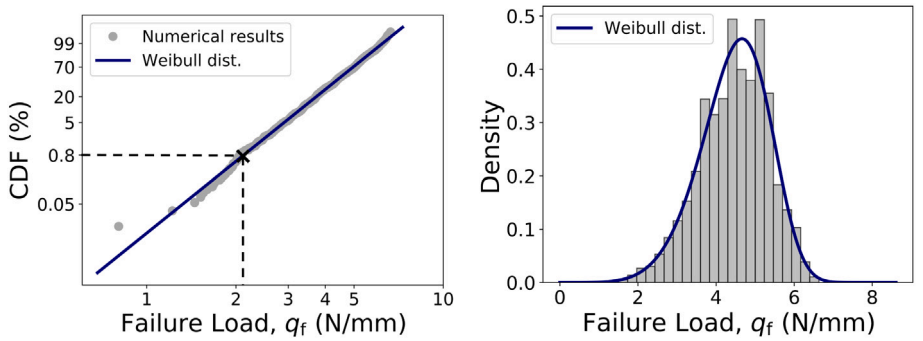

Fig. 20. Weibull distribution of the failure load for the simply supported beam under uniformly distributed load: (a) Linearized cumulative distribution function; (b) Probability density function.

Fig. 11(a)), the glass tensile strength evaluated with a 0.8% probability of failure is $\sigma_{f,0.008} = 20.96$ MPa. As a consequence, the resistant bending moment is:

$$M_{z;R} = \frac{\sigma_{f,0.008} I}{y_{max}} = 196.50 \text{ N mm} \tag{32}$$

being I the second moment of area and y_{max} the distance from the neutral axis to the most extreme fibre. Finally, the load bearing capacity is obtained as follows:

$$P_R = \frac{4M_{z;R}}{L} = 26.20 \text{ N} \tag{33}$$

Therefore, it can be concluded that the load bearing capacity estimated with the proposed probabilistic FEM approach is 43% greater than the one evaluated with the stress-based approach. The difference in load-carrying capacity prediction is due to the fact that the stress-based design approach assumes that the point of origin of failure coincides with the point of maximum stress, that, in most of the cases, does not occur [18]. In that regard, the distribution in Fig. 18 shows that the point of the origin of failure matches with the point of maximum stress in less than one case out of five.

6.3. Edge-cracked simply supported beam under uniformly distributed load

The cracked beam of Section 6.1 is now simply supported and subjected to a uniformly distributed load as shown in Fig. 19. As in the previous case studies, the size a of the cracks follows the Pareto distribution with $a_0 = 0.02$ mm and $c = 3$.

Figs. 20 and 21 show the sampling probability distributions of the failure load q_f and critical edge crack size a_c, which are well fitted by the Weibull and Fréchet distributions, respectively. The Weibull and Fréchet parameters were determined using the sample mean and variance by means of the moments method as explained before. Their values are: $\hat{\theta} = 4.8$ N/mm and $\hat{\beta} = 5.9$, $\hat{\lambda} = 2.3 \times 10^{-4}$ and $\hat{\alpha} = 2.8$.

As shown in Fig. 22, the coordinate x of the critical crack follows the Gaussian distribution with mean $\bar{x} = 15$ mm and standard deviation $\sqrt{s_x^2} = 7$ mm.

The load bearing capacity of the beam under uniformly distributed load obtained from the Weibull diagram (Fig. 20) for the 0.8% probability of failure is $q_{f,0.008} = 2.12$ N/mm. This value is compared with that estimated using the stress-based failure criterion.

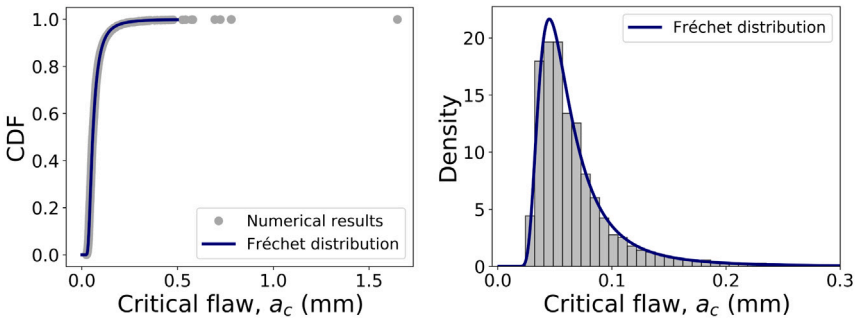

Fig. 21. Fréchet distribution of the critical edge crack size for the simply supported beam under uniformly distributed load: (a) Cumulative distribution function (CDF); (b) Probability density function.

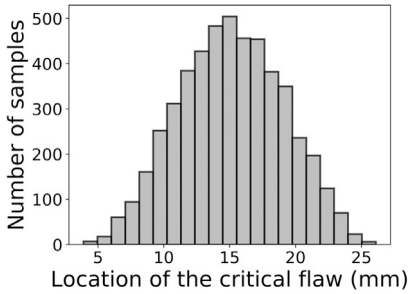

Fig. 22. Location of the critical edge crack for the simply supported beam under uniformly distributed load.

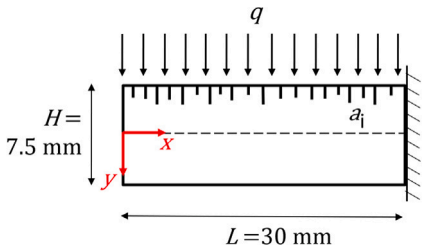

Fig. 23. Sketch of the cantilever beam test.

As obtained above (see Section 6.2), the resistant bending moment of the glass beam is $M_{z;R}$ = 196.50 N mm. Therefore, the load carrying capacity calculated with the stress-based failure criterion is:

$$q_R = \frac{8M_{z;R}}{L^2} = 1.75 \text{ N/mm} \tag{34}$$

In conclusion, the load bearing capacity assessed using the proposed probabilistic FEM approach is 21% larger than that obtained using the stress-based failure criterion.

6.4. Edge-cracked cantilever beam under uniformly distributed load

The last example involves a cantilever beam subjected to a uniformly distributed load (Fig. 23). As in the previous cases, the beam contains 29 cracks, whose size a is Pareto distributed ($a_0 = 0.020$ mm and $c = 3.0$).

The Weibull distribution of the failure load interpolates $N = 5000$ different points ($q_{f,i}$, $\hat{G}_i$) in Fig. 25. Each $q_{f,i}$ value is obtained using the K_I-based fracture criterion. Fig. 24 depicts the K_I distribution along the beam for a single FEM simulation. Near the fixed end of the beam, where the bending moment is the largest, the highest K_I values are found.

The sampling probability distribution of the critical edge crack size is fitted with the Fréchet distribution in Fig. 26. The estimated Weibull and Fréchet distribution parameters are: $\hat{\theta} = 1.8$ N/mm and $\hat{\beta} = 6.0$, $\hat{\lambda} = 1.6 \times 10^{-4}$ and $\hat{\alpha} = 2.7$. The point of origin of failure is located between $x = 15$ mm and $x = 30$ mm, as shown in Fig. 27.

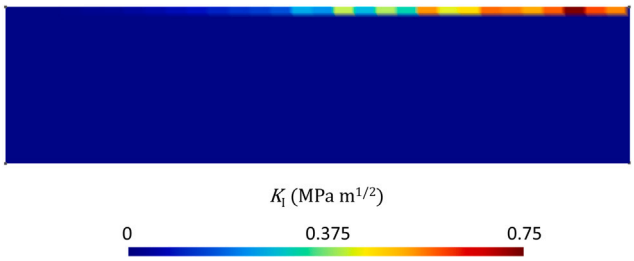

Fig. 24. K_I values at the crack tips for a single simulation of the cantilever beam under uniformly distributed load.

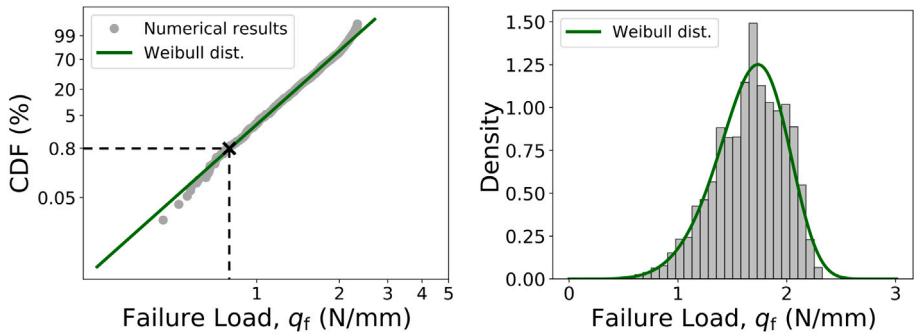

Fig. 25. Weibull distribution of the failure load for the cantilever beam under uniformly distributed load: (a) Linearized cumulative distribution function; (b) Probability density function.

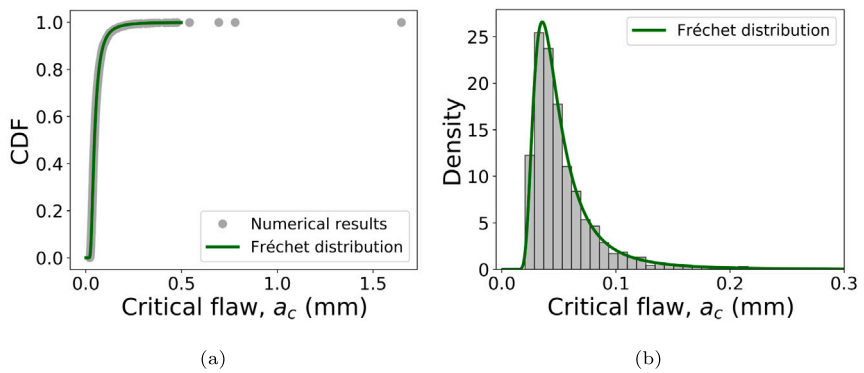

Fig. 26. Fréchet distribution of the critical edge crack size for the cantilever beam under uniformly distributed load: (a) Cumulative distribution function (CDF); (b) Probability density function.

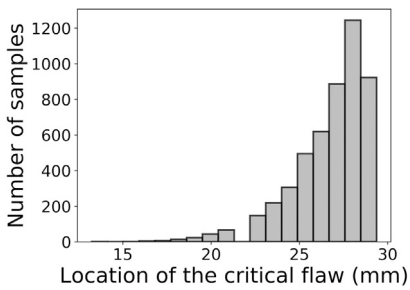

Fig. 27. Location of the critical edge crack for the cantilever beam under uniformly distributed load.

The load resistance of the cantilever beam evaluated with the stress-based failure criterion is:

$$q_R = \frac{2M_{z;R}}{L^2} = 0.44 \text{ N/mm} \tag{35}$$

whereas the load bearing capacity obtained with the proposed probabilistic approach is $q_{f,0.008} = 0.80$ N/mm (see Fig. 25(a)). Therefore, the K_I-based prediction is 83% larger than the stress-based prediction.

7. Conclusions

A new probabilistic FEM approach has been proposed for the design of structural glass elements and, more generally, brittle materials such as ceramics and polysilicon micro-structures. In the current version, the methodology, which adopts a stress intensity factor-based fracture criterion and makes use of the Monte Carlo simulation to predict the failure load associated to a chosen probability of failure, can be applied to plane stress/strain problems, with arbitrary geometries, boundary conditions and flaw size statistical distributions. Moreover, it has the capability to take into account the interaction among cracks and the effect of stress concentrations on the stress intensity factor.

Advantages of the proposed procedure are an increased reliability of the design process and a more accurate prediction of the load bearing capacity compared to the stress-based design approach. With reference to the considered case studies, the developed method provided load carrying capacities larger than the predictions of the stress-based approach by an extent variable between 21% and 83%, depending on the stress gradient within the glass specimen.

In this first version, deterministic assumptions have been done on the crack position, the crack density, and the statistical distribution of the edge flaws. However, the crack density and the statistical distribution of the cracks could be evaluated, within confidence intervals, by means of experimental tests, while the crack position could be selected randomly from a statistical distribution. To quantify how the uncertainties on these three parameters affect the output variable, a sensitivity analysis will be carried out in future work. Besides, the extension of the methodology to 3D problems will be pursued, to generalize the method and to better investigate the effect of shape, orientation and location of the cracks, all factors that influence the distribution function of the glass strength.

CRediT authorship contribution statement

Gregorio Mariggiò: Writing – original draft, Software, Investigation, Formal analysis. **Giulio Ventura:** Writing – review & editing, Software, Funding acquisition. **Mauro Corrado:** Writing – review & editing, Supervision, Methodology, Conceptualization.

Declaration of competing interest

The authors declare that they have no known competing financial interests or personal relationships that could have appeared to influence the work reported in this paper.

Data availability

Data will be made available on request.

Acknowledgements

The support from the Italian Ministry of University and Research (MUR) to the research project “XFAST-SIMS: Extra fast and accurate simulation of complex structural systems” (Grant agreement n. 20173C478N) is gratefully acknowledged. The authors are also grateful to the support provided by Politecnico di Torino, Italy, through the diffuse research grant initiative.

References

[1] Kinsella DT, Persson K. An analysis of glass fracture statistics, vol. 6. Challenging Glass 6; 2018.
[2] Vandebroek M, Belis J, Louter C, Caspeele S. Influence of the load history on the edge strength of glass with arrised and ground edge finishing. Eng Fract Mech 2013;104:29–40.
[3] Mariggiò G, Dalle Vacche S, Bongiovanni R, Louter C, Corrado M. A durable coating to prevent stress corrosion effects on the surface strength of annealed glass. Glass Struct Eng 2021;6:449–62.
[4] Mariggiò G, Dalle Vacche S, Bongiovanni R, Louter C, Corrado M. Enhancing the design bending strength of new and aged glass with a functional coating. Glass Struct Eng 2020;5:135–46.
[5] Pisano G, Bonati A, Royer-Carfagni G. The effect of size and stress state on the strength of architectural glass. Experiments versus theory. Constr Build Mater 2021;283:122635.
[6] Papadopoulos N, Drosou C. Influence of weather conditions on glass properties. J Univ Chem Technol Metall 2012;47:429–39.
[7] Kleuderlein J, Ensslen F, Schneider J. Study on edge strength of float glass as a function of edge processing. Stahlbau 2016;85:149–59.
[8] Müller-Braun S, Seel M, König M, Hof P, Schneider J, Oechsner M. Cut edge of annealed float glass: crack system and possibilities to increase the edge strength by adjusting the cutting process. Glass Struct Eng 2020;5:3–25.
[9] Vocialta M, Corrado M, Molinari J-F. Numerical analysis of fragmentation in tempered glass with parallel dynamic insertion of cohesive elements. Eng Fract Mech 2018;188:448–69.
[10] Griffith AA. The phenomena of rupture and flow in solids. Phil Trans R Soc A 1921;221(582–593):163–98.

[11] Schneider J, Schula S, Weinhold WP. Characterisation of the scratch resistance of annealed and tempered architectural glass. Thin Solid Films 2012;520(12):4190–8.
[12] Schula S, Schneider J, Vandebroek M, Belis J. Fracture strength of glass, engineering testing methods and estimation of characteristic values. In: Belis J, Louter C, Mocibob D, editors. COST action TU0905, mid-term conference on structural glass, proceedings. Taylor & Francis Group; 2013, p. 223–34.
[13] EN 16612:2019. Glass in building - Determination of the lateral load resistance of glass panes by calculation. Brussels: European Committee for Standardization; 2019.
[14] CEN/TS 19100-1. Design for glass structures – Part 1: Basis of design and materials. Brussels: European Standard, European Committee for Standardization (CEN); 2021.
[15] EN 1288-2:2000. Glass in building - Determination of bending strength of glass - Part 2: Coaxial double ring test on flat specimens with large test surface areas. Brussels: European Committee for Standardization; 2000.
[16] Afferrante L, Ciavarella M, Valenza E. Is Weibull's modulus really a material constant? Example case with interacting collinear cracks. Int J Solids Struct 2006;43(17):5147–57.
[17] Kulhawy FH, Phoon K. Engineering judgment in the evolution from deterministic to reliability-based foundation design. In: Shackelford C, Nelson P, Roth M, editors. Proceedings of uncertainty 1996, uncertainty in the geologic environment - from theory to practice (GSP 58). New York: ASCE; 1996.
[18] Overend M, Parke GAR, Buhagiar D. Predicting failure in glass—A general crack growth model. J Struct Eng 2007;133:1146–55.
[19] Ballarini R, Pisano G, Royer Carfagni G. New calibration of partial material factors for the structural design of float glass. Comparison of bounded and unbounded statistics for glass strength. Constr Build Mater 2016;121:69–80.
[20] Lamela MJ, Ramos A, Fernández P, Fernández-Canteli A, Przybilla C, Huerta C, et al. Probabilistic characterization of glass under different type of testing. Procedia Mater Sci 2014;3:2111–6, 20th European Conference on Fracture.
[21] ASTM E1300-16. Standard practice for determining load resistance of glass in buildings. American Society for Testing Materials; 2016.
[22] Beason WL. A Failure prediction model for window glass. Texas Tech University; 1980.
[23] Beason WL, Morgan JR. Glass failure prediction model. J Struct Eng 1984;110(2):197–212.
[24] Weibull W. A statistical theory of the strength of materials. In: Proceedings of the Royal Swedish Academy of Engineering. 1939.
[25] Nategh S, Missinne J, Vijverman P, Van Steenberge G, Belis J. Effect of ultrashort laser-induced surface flaws on architectural glass strength. Constr Build Mater 2021;295:123590.
[26] Sakata Y, Terasaki N, Nonaka K. Development of a novel non-contact inspection technique to detect micro cracks under the surface of a glass substrate by thermal stress-induced light scattering method. Opt Laser Technol 2017;90:80–3.
[27] Pan Z, Yang J, Wang X, Wang F, Azim I, Wang C. Image-based surface scratch detection on architectural glass panels using deep learning approach. Constr Build Mater 2021;282:122717.
[28] Lindqvist M, Vandebroek M, Louter C, Belis J. Influence of edge flaws on failure strength of glass. In: Glass performance days. 2011, p. 126–9.
[29] Vandebroek M, Belis J, Louter C, Van Tendeloo G. Experimental validation of edge strength model for glass with polished and cut edge finishing. Eng Fract Mech 2012;96:480–9.
[30] Belytschko T, Gracie R, Ventura G. A review of extended/generalized finite element methods for material modeling. Modelling Simul Mater Sci Eng 2009;17(4):043001.
[31] Irwin GR. Analysis of Stresses and Strains Near the End of a Crack Traversing a Plate. J Appl Mech 1957;24(3):361–4.
[32] Mencik J. Strength and fracture of glass and ceramics, glass science and technology, vol. 12. Amsterdam: Elsevier; 1992.
[33] Tada H, Paris PC, Irwin GR. The stress analysis of cracks handbook. The American Society of Mechanical Engineers Press; 2000.
[34] Yankelevsky DZ. Strength prediction of annealed glass plates – A new model. Eng Struct 2014;79:244–55.
[35] Kinsella DT, Persson K. A numerical method for analysis of fracture statistics of glass and simulations of a double ring bending test. Glass Struct Eng 2018;3:139–52.
[36] Poloniecki J, Wilshaw T. Determination of surface crack size densities in glass. Nature (Phys Sci) 1971;229:226–7.
[37] Poloniecki J. Statistical investigation of surface flaws [Ph.D. thesis], The University of Sussex; 1974.
[38] Tandon R, Paliwal B, Gibson C. Practical aspects of using Hertzian ring crack initiation to measure surface flaw densities in glasses: influence of humidity, friction and searched areas. Phil Mag 2013;93:2847–63.
[39] Belytschko T, Black T. Elastic crack growth in finite elements with minimal remeshing. Internat J Numer Methods Engrg 1999;45(5):601–20.
[40] Moës N, Dolbow J, Belytschko T. A finite element method for crack growth without remeshing. Internat J Numer Methods Engrg 1999;46(1):131–50.
[41] Fries T-P, Belytschko T. The extended/generalized finite element method: an overview of the method and its applications. Internat J Numer Methods Engrg 2010;84(3):253–304.
[42] Liu XY, Xiao QZ, Karihaloo BL. XFEM for direct evaluation of mixed mode SIFs in homogeneous and bi-materials. Internat J Numer Methods Engrg 2004;59(8):1103–18.
[43] Karihaloo BL, Xiao QZ. Direct evaluation of accurate SIF with PUM. In: 10th international conference on fracture - ICF10. Advances in fracture research, 2001.
[44] Benvenuti E, Ventura G, Ponara N. Finite element quadrature of regularized discontinuous and singular level set functions in 3D problems. Algorithms 2012;5(4):529–44.
[45] Benvenuti E, Ventura G, Ponara N, Tralli A. Variationally consistent extended FE model for 3D planar and curved imperfect interfaces. Comput Methods Appl Mech Engrg 2013;267:434–57.
[46] Ventura G, Moran B, Belytschko T. Dislocations by partition of unity. Internat J Numer Methods Engrg 2005;62(11):1463–87.
[47] Albinmousa J, Merah N, Khan S. A model for calculating geometry factors for a mixed-mode I–II single edge notched tension specimen. Eng Fract Mech 2011;78(18):3300–7.
[48] Ventura G. On the elimination of quadrature subcells for discontinuous functions in the eXtended Finite-Element Method. Internat J Numer Methods Engrg 2006;66:761–95.
[49] Ventura G, Benvenuti E. Equivalent polynomials for quadrature in Heaviside function enriched elements. Internat J Numer Methods Engrg 2015;102:688–710.
[50] Mariggiò G, Fichera S, Corrado M, Ventura G. EQP - A 2D/3D library for integration of polynomials times step function. SoftwareX 2020;12:100636.
[51] Ventura G, Gracie R, Belytschko T. Fast integration and weight function blending in the extended finite element method. Internat J Numer Methods Engrg 2009;77(1):1–29.
[52] Fries T-P. A corrected XFEM approximation without problems in blending elements. Internat J Numer Methods Engrg 2008;75(5):503–32.
[53] Auradou H, Vandembroucq D, Guillot C, Bouchaud E. A probabilistic model for the stress corrosion fracture of glass. In: Transactions, SMiRT 16. Washington DC; 2001.
[54] Jiang ZD, Zeghloul A, Bezine G, Petit J. Stress intensity factors of parallel cracks in a finite width sheet. Eng Fract Mech 1990;35(6):1073–9.
[55] Forbes C, Evans M, Hastings N, Peacock B. Statistical distributions. 4th ed. Wiley; 2010.
[56] Haldimann M. Fracture strength of structural glass elements – Analytical and numerical modelling, testing and design [Ph.D. thesis], Lausanne, Switzerland: École Polytechnique Fédérale de Lausanne; 2006.
[57] Ramos P, Louzada F, Ramos E, Dey S. The Fréchet distribution: Estimation and application an overview. J Stat Manag Syst 2020;23:549–78.
[58] Kotz S, Nadarajah S. Extreme value distributions: Theory and pubblications. London: Imperial College Press; 2000.
[59] Haldimann M, Luible A, Overend M. Structural use of glass. Zurich: International Association for Bridge and Structural Engineering IABSE; 2008.
[60] García O. Simplified method-of-moments estimation for the Weibull distribution. N Z J For Sci 1981;11:304–6.
[61] Ballarini R, Pisano G, Royer-Carfagni G. The lower bound for glass strength and its interpretation with generalized Weibull statistics for structural applications. J Eng Mech 2016;142(12):04016100.